Article:
Taima, M.S., El-Sayed, T.A., Shehab, M.B. et al. (2023) Vibration analysis of cracked beam based on Reddy beam theory by finite element method. Journal of Vibration and Control, 29 (19-20). pp. 4589-4606. ISSN: 1077-5463

https://doi.org/10.1177/10775463221122122

Vibration Analysis of Cracked Beam Based on Reddy Beam Theory by Finite Element Method

Moustafa S. Taima[a], T.A. El-Sayed[a,b,*], Mohamed B. Shehab[a], Said H. Farghaly[a], Russell J. Hand[c]

[a]*Department of Mechanical Design, Faculty of Engineering, Mataria, Helwan University, P.O. Box 11718, Helmeiat-Elzaton, Cairo, Egypt*
[b]*Centre for Applied Dynamics Research, School of Engineering, University of Aberdeen, Aberdeen, AB24 3UE, UK*
[c]*Department of Materials Science and Engineering, University of Sheffield, Sir Robert Hadfield Building, Mappin Street, Sheffield S1 3JD, UK*

Abstract

The lateral vibration of cracked isotropic thick beams is investigated. Generally, the analysis of thick beam based on line elements can be undertaken using either Timoshenko beam theory or a third order beam theory (TSDT) such as Reddy beam theory. TSDT is superior to Timoshenko beam theory, as it eliminates the need for a shear correction coefficient. However, there is no available solution for a cracked beam based on Reddy beam theory which is main focus of this paper. The investigated beam is divided into several elements where their stiffness and mass matrices are derived using Reddy beam theory. Each element has two nodes with 3 degrees of freedom (1 lateral and 2 rotational) at each node. The crack was modeled using two rotating springs with stiffnesses that varied with crack depth. These elements are used to connect the adjacent beam elements. The impact of boundary conditions, slenderness ratio, crack location, and crack depth are investigated. In addition, experimental and finite element analyses of cracked steel beams is undertaken to validate the results of the present model. The results show that the maximum deviation between the analytical and the experimental results is less than 3 % up to the third mode shape.

Keywords: Reddy beam theory, finite element, lateral vibration, experimental analysis, cracked beam.

1. Introduction

Cracks in vibrating components may cause catastrophic failures. As a result, detecting cracks and understanding their consequences for a structure is critical for safety. The major issue is how to detect the presence of such crack, as well as its position and depth in a structural member, before failure occurs, so that necessary actions can be implemented to prevent further damage.

Dimarogonas (1996) surveyed a range of strategies that are used for diagnosis of cracks. Non-destructive testing (NDT) methods that are used to detect defects include visual inspection, ultrasonic testing, thermography, radiography, electromagnetic testing, acoustic emission, and stereography (Dwivedi et al., 2018). Most of these methods require access to the damaged section so that such sites can be directly scanned. Vibration-based methods are a viable

*Corresponding author
Email addresses: moustafa.samir@m-eng.helwan.edu.eg (Moustafa S. Taima), tamer.elsayed@abdn.ac.uk (T.A. El-Sayed), mohamed.bakry@m-eng.helwan.edu.eg (Mohamed B. Shehab), said.farghaly@m-eng.helwan.edu.eg (Said H. Farghaly), r.hand@sheffield.ac.uk (Russell J. Hand)

substitute for traditional NDT methods. Vibration-based methods have a number of specific advantages: most notably the test equipment is relatively inexpensive; the vibration data may be gathered from a single location or from many locations on the structural component, and access to the damaged section is not necessary (Sánchez et al., 2016). The presence of crack in a structural part causes local flexibility that varies with crack depth. The crack depth and location affect the properties of a structure including the natural frequency, the vibration response amplitude, and the mode shape. These changes in the structure dynamical properties can be easily measured, and therefore a number of papers have focused on the analysis of cracked beams (Ahmed and Uddin, 2019; Aria et al., 2019; Banerjee and Guo, 2009; Ebrahimi et al., 2005; Farghaly, 1994; Kim et al., 2018; Kisa et al., 1998; Labib et al., 2014; Loya et al., 2009; Mazaheri et al., 2018; Torabi and Nafar Dastgerdi, 2012; Yamuna and Sambasivarao, 2014; Yang et al., 2015; Yendhe et al., 2016) and this is also the aim of this paper.

The advantage of analytical methods is that they enable the derivation of models that can correlate the observed dynamic features with the crack parameters. These models can then be used to solve the inverse problem of crack detection based on measured responses or natural frequencies. Characterization of the dynamic response of damaged beams leads to greater insight into damage identification via solution of the inverse problem based on experimental measurements. Friswell (2007) provided an overview on using measured data for damage identification (position and size). Damage detection inverse problems combine experimental dynamic measured data with data obtained from an initial numerical model to improve the model. The first stage in detecting damage is to define a reliable model that is compatible with the real structure and to evaluate a correct solution to the direct problem. Studies, such as (Dilena et al., 2011; Morassi, 2001; Vestroni and Capecchi, 2000), have employed inverse analysis based on the fluctuation of natural frequencies caused by the presence of a single damage feature (crack size and position). There are also some studies that have looked at the detection of multiple cracks based on measurements of the natural frequencies (Luo and Hanagud, 1997; Patil and Maiti, 2005; Xiaoqing et al., 2010).

Beams are fundamental structural elements that are used to transfer lateral loads in many engineering applications including long-span bridges, buildings, turbomachine blades, aircraft wings, robot arms, etc. Several theories have been formulated to describe the lateral vibrations of beams namely the Bernoulli-Euler, Rayleigh, Timoshenko, Levinson and Reddy theories (Wang et al., 2000). Each of these theories has its own advantages and disadvantages.

Bernoulli-Euler (or classical) beam theory (CBT) is the simplest and oldest theory, which is still widely used for thin beams. In CBT, the plain section is assumed to remain planar and perpendicular to the beam axis after deformation, as shown in Fig.1-b. This theory neglects transverse shear deformation, which is less of an issue for thin beams, hence its continued use in such cases. The significance of shear deformations in elastic beams was first demonstrated by Timoshenko (1921) and Timoshenko beam theory can be considered as a first-order shear deformation theory (FSDT). Timoshenko beam theory is widely used for thick beams (Cheng et al., 2011; El-Sayed and El-Mongy, 2021; El-Sayed and Farghaly, 2018, 2020; Elsawaf et al., 2020; Farghaly and El-Sayed, 2016, 2017; Kaya and Dowling,

2016; Yardimoglu, 2010) . In this case a plane section again remains plane after deformation, as shown in Fig.1-c, however the assumption that the plane remains perpendicular to the beam axis is relaxed. The drawback of this theory is that the shear distribution across the beam section is incorrectly assumed to be uniform, although this can be compensated by using a shear correction factor. This drawback of FSDT motivated the development of higher-order shear deformation theories (HSDTs) first introduced by Levinson (1981). Basically, in HSDTs, the considered displacement field eliminates the transverse shear strain and stress on the top and bottom planes of the beam (Bickford, 1982; Heyliger and Reddy, 1988; Huang et al., 2013; Jemielita, 1975; Levinson, 1980, 1981; Reddy, 1984a,b). Reddy beam theory or third-order shear deformation theory (TSDT) is one of the most popular HSDTs, with still high order theories higher being rarely used because the additional gains in accuracy achieved are too low. TSDT assumes a parabolic distribution of the transverse shear strain and stress with respect to the thickness coordinate, as shown in Fig.1-d. Note that the beam cross-section is allowed to warp in such a way that it remains normal to the beam shear-free surfaces.

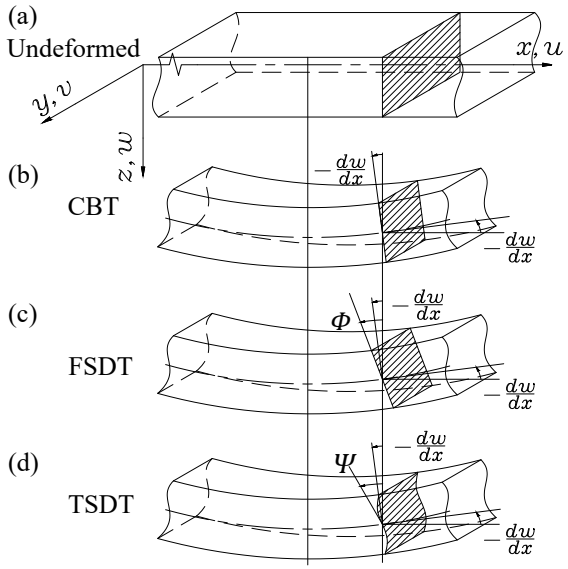

Figure 1: Coordinate system and deformation of a cross-sectional plane in different beam theories (Wang et al., 2000)

Heyliger and Reddy (1988) developed a finite element model based on linear and non-linear TSDT. They presented several examples comparing TSDT results with the previous results to show the theory's accuracy and examined the effect of the slenderness ratio and different boundary conditions. Soldatos and Sophocleous (2001) introduced a general beam theory that includes CBT, FSDT and TSDT. They analytically derived frequency equations and the natural frequencies for different boundary conditions. Şimeşk and Kocatürk (2007) employed Lagrange multipliers to satisfy several boundary conditions based on TSDT. They examined different beam aspect ratios and compared their results with CBT and FSDT. Yesilce and Catal (2009) studied the free vibration of an axially loaded beam on elastic soil using the differential transform method (DTM) based on TSDT and compared the natural frequencies of clamped-simply supported beams with the analytical solutions. The authors examined the effects of relative stiffness,

stiffness ratio and dimensionless axial force. Bozyigit and Yesilce (2016) investigated axially moving beams using the dynamic stiffness method (DSM) and DTM according to TSDT. They studied the effect of dimensionless axial speed and force for different boundary conditions. The results show that the obtained natural frequencies from DTM and DSM are in very good agreement with the analytical results. They concluded that increasing the axial speed with constant axial tensile force decreases the natural frequencies for all boundary conditions and vice versa.

The vibration analysis of composite beams has been reported in a range of literature. For example the behavior of sandwich composite beams as a function of different boundary conditions, laminate schemes and aspect ratios was reported in (Khdeir and Reddy, 1994; Marur and Kant, 1996). Khdeir and Reddy (1994) applied a general beam theory to study a cross-ply rectangular beam with arbitrary boundary conditions. Their study showed that the results based on the different shear deformation theories were very close together, with the largest deviation in the results being between the shear theories and Bernoulli-beam theory. Marur and Kant (1996) used a finite element model in conjunction with three different HSDTs to present the free vibration analysis of sandwich and composite beams. The authors compared the results of the three theories with the first order shear theory and with their results to determine the most effective method. Jun et al. (2009) introduced TSDT using the dynamic stiffness method. They also examined the influences of Poisson's ratio, material anisotropy, slenderness and boundary condition on the natural frequencies of the beams. Karamanlı (2018) investigated two-directional functionally graded beams using TSDT. The equations of motion were derived by means of Lagrange equations in conjunction with auxiliary polynomials. The author examined the influence of the different gradient indexes, various aspect ratios and boundary conditions on the results. Wattanasakulpong et al. (2018) investigated functionally graded porous beams using TSDT. Both beam ends were supported by rotational and translational springs and the Chebyshev collocation method was applied to solve the governing equations.

Yesilce and Catal (2011) studied the free vibration analysis of beams with variable cross-section rested on elastic soil with/without axial forces using DTM based on TSDT. Parameters for the relative stiffness, stiffness ratio and a dimensionless multiplication factor for the axial compressive force were incorporated into the equations of motion in order to investigate their effects on the natural frequencies. The results were compared with the results of the analytical solution where a very good agreement was observed. They concluded that increasing the axial compressive force leads to reduction in natural frequency unlike increasing the relative stiffness and the stiffness ratio which leads to increasing in natural frequency. Yesilce (2011) investigated the free vibration analysis of multi-span beams carrying multiple spring-mass systems based on TSDT. They used the exact solutions for the natural frequencies and mode shapes. The natural frequencies were calculated by using the numerical assembly technique and the secant method and the effects of attached spring-mass systems on the free vibration characteristics of the 1–4 span beams were studied.

Yamuna and Sambasivarao (2014) investigated the natural frequency of a simply supported beam with a triangular

crack using ANSYS finite element software. The effect of using different crack locations was considered, and the results were compared to those for an uncracked beam. The results show that the 1st natural frequency of a beam without cracks is higher than that for the same beam with cracks. Additionally, when the crack location moves from either end to the center of the beam the first natural frequency decreases. Ahmed and Uddin (2019) studied the vibrational analysis of a cracked I beam subjected to periodic loading using 'ABAQUS CAE' finite element software. They analyzed the behavior of natural frequency for various parameters such as crack position, crack depth, crack opening and mesh sensitivity. The results of the study show that the presence of a crack reduces the natural frequency depending on the crack position and its depth. The significance of vibration analysis is clear when the crack reaches the web of the I beam. Furthermore, if the crack depth is greater or the position of the crack is closer to the fixed end, the resonance occurs earlier. Yendhe et al. (2016) investigated the vibration behavior of beams both experimentally and using ANSYS. They investigated beams with rectangular cross-sections with and without cracks. The depth of the crack and its location and different boundary conditions were used as variable parameters. The results demonstrate that the change in frequencies is affected not only by crack depth and crack location, but also by the mode number. The effect of a crack is greater for a crack located where the bending moment is higher (i.e. the centerline for a simply supported beam and the fixed end for a cantilever beam). Ebrahimi et al. (2005) studied the bending vibration of a uniform simply supported Bernoulli-Euler beam with an open edge crack using Hamilton's principle. The results show that increasing crack depth reduces natural frequencies. Moving the crack location towards the center of the beam, results in increasing the rate of change in the first natural frequency. However, this is not valid for the other higher natural frequencies. The validity of the obtained results has been confirmed by comparison with the finite element results. Kim et al. (2018) examined the free vibration behavior of a cracked Timoshenko beam model based on ultra-spherical polynomials for general boundary conditions modeled using elastic springs at both ends. Yang et al. (2015) investigated the free vibration of rectangular cracked Bernoulli-Euler beam made of functionally graded materials (FGMs) using the transfer matrix method (TMM). Much research work considers the free vibration analysis of cracked beams using Bernoulli-Euler (Aria et al., 2019; Banerjee and Guo, 2009; Labib et al., 2014; Loya et al., 2009; Mazaheri et al., 2018) and Timoshenko(Farghaly, 1994; Kisa et al., 1998; Torabi and Nafar Dastgerdi, 2012) theories, leading to the conclusion that the presence of a crack reduces the natural frequency of vibration. Also, a number of papers have investigated the free vibration of discontinuous beams and frames without subdivision into sub-elements, which restricted the degrees of freedom to the overall system. Caddemi and Caliò (2009) investigated the vibration modes of a Bernoulli Euler beam with multiple open cracks. They modeled the open cracks as a sequence of generalized Dirac delta functions, without enforcement of any continuity conditions and employed the dynamic stiffness matrix in vibration analysis of frame structures with multiple cracks. Caddemi and Caliò (2013) developed a finite element model of a stepped Timoshenko beam for the dynamic analysis of frame structures with deflection, rotation, and abrupt cross-sectional fluctuations. Their approach was based on the use of Heaviside and Dirac delta

distributions to represent abrupt discontinuities in the beam. Caddemi and Morassi (2013) proposed a mathematical model for multiply cracked Bernoulli Euler beams, in which they justified using the rotating elastic spring model to represent an open crack. Caddemi et al. (2017) used the dynamic stiffness matrix for modeling the axially loaded frames with arbitrary number of open cracks. The size of their DSM remained constant regardless of the number of cracks along the beam.

From the previous literature we can conclude that the TSDT has an advantage over Timoshenko beam theory in that it does not require the evaluation of a shear coefficient κ with changing beam cross section (Cowper, 1966; Timoshenko, 1921). A solution for the case of a cracked thick beam has not been published yet and this is aim of the current paper. In Section 2 the theoretical model based on TSDT is investigated and the crack model is discussed, along with finite element analysis using ANSYS and the experimental setup used for the verification of the model. The model results and verifications are presented in Section 3. Finally, the main outcomes and conclusions are presented in Section 4.

2. Theoretical model and experimental setup

The Cartesian coordinate system is used to describe the Reddy beam element as shown in Fig.1-(a). The (x, y, z) axes are placed along the beam length L, width W and thickness (height) h respectively. The displacements along the (x, y, z) coordinate directions are (u, v, w) respectively. In the current analysis, and for simplicity, the transverse vibration in y direction is not considered hence the v displacement is assumed to be zero. A Reddy beam with total length L and uniform cross-section area $A = W \times h$ is shown in Fig.2. The beam has a transverse through edge crack of depth a at a position L_c. The beam is connected to masses at both ends by transverse and rotational springs and concentrated masses are attached to the beam at both ends. The beam is subject to a non-uniform distributed transverse force $f(x)$.

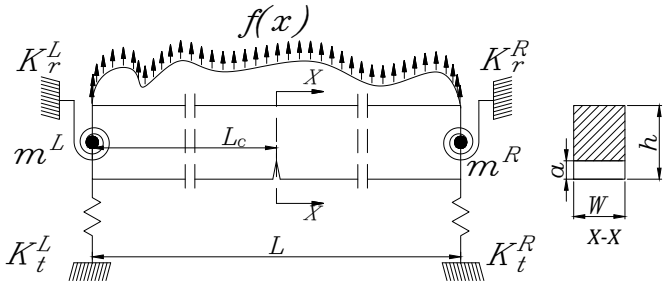

Figure 2: Cracked Reddy beam attached by transverse and rotational springs to masses at both ends and loaded by a non-uniform distributed transverse force.

2.1. Governing equations

The displacement field according to TSDT is given by

$$\begin{aligned} u(x,z) =& z\psi - \frac{4}{3h^2}z^3\left(\psi + \frac{\mathrm{d}w}{\mathrm{d}x}\right), \\ w(x,z) =& w, \end{aligned} \tag{1}$$

where ψ is the value of the slope$\varphi(x,z,t)$ given by

$$\varphi = \frac{\partial u}{\partial z} = \psi - \frac{4}{h^2}z^2\left(\psi + \frac{\mathrm{d}w}{\mathrm{d}x}\right), \tag{2}$$

at $z = 0$, as shown in Fig.1-(d).

The average value of the slope over the interval $z \in [-h/2\,, h/2\,]$ is given by

$$\varphi_{av} = \frac{\int_{-\frac{h}{2}}^{\frac{h}{2}} \varphi \mathrm{d}z}{h} = \frac{\left[z\,\psi - \frac{4}{3h^2}z^3\left(\psi + \frac{\mathrm{d}w}{\mathrm{d}x}\right)\right]_{-\frac{h}{2}}^{\frac{h}{2}}}{h} = \frac{2}{3}\psi - \frac{1}{3}\frac{\mathrm{d}w}{\mathrm{d}x} \tag{3}$$

Here, the obtained value of φ_{av} is used to evaluate the torsional spring moment at the beam boundaries and intermediate nodes. The same concept is used with crack equivalent torsional spring. Then, the moment resulting from a torsional spring K_r can be written as shown in Eq. (4). This moment can be divided into two components written in terms of ψ and $\frac{\mathrm{d}w}{\mathrm{d}x}$.

$$F_r = K_r\varphi_{av} = K_r\left(\frac{2}{3}\psi - \frac{1}{3}\frac{\mathrm{d}w}{\mathrm{d}x}\right) = K_\psi\psi - K_\theta\frac{\mathrm{d}w}{\mathrm{d}x}, \tag{4}$$

where F_r is the total rotational moment, $K_\psi = \frac{2}{3}K_r$ and $K_\theta = \frac{1}{3}K_r$.

The strain and stress components corresponding to the displacement field given by Eq.(1) are:

$$\begin{aligned} \varepsilon_{xx} =& \frac{\partial u}{\partial x} = \left(z\frac{\mathrm{d}\psi}{\mathrm{d}x} - \frac{4}{3h^2}z^3\left(\frac{\mathrm{d}\psi}{\mathrm{d}x} + \frac{\mathrm{d}^2w}{\mathrm{d}x^2}\right)\right), \\ \gamma_{xz} =& \frac{\partial u}{\partial z} + \frac{\partial w}{\partial x} = \left(1 - \frac{4}{h^2}z^2\right)\left(\psi + \frac{\mathrm{d}w}{\mathrm{d}x}\right), \end{aligned} \tag{5}$$

$$\begin{aligned} \sigma_{xx} =& E\varepsilon_{xx} = E\left(z\frac{\mathrm{d}\psi}{\mathrm{d}x} - \frac{4}{3h^2}z^3\left(\frac{\mathrm{d}\psi}{\mathrm{d}x} + \frac{\mathrm{d}^2w}{\mathrm{d}x^2}\right)\right), \\ \tau_{xz} =& G\gamma_{xz} = G\left(1 - \frac{4}{h^2}z^2\right)\left(\psi + \frac{\mathrm{d}w}{\mathrm{d}x}\right), \end{aligned} \tag{6}$$

where E and G are the Young's and shear moduli of the beam respectively.

The strain energy of the system Π can be expressed as the sum of the strain energy of the beam element

$$\Pi_1 = 1/2\int_A\int_0^L (\sigma_{xx}\varepsilon_{xx} + \tau_{xz}\gamma_{xz})\,\mathrm{d}x\,\mathrm{d}A, \tag{7}$$

and the strain energy at the beam element boundaries

$$\Pi_2 = \left[\frac{1}{2}\left(K_t^L w^2 + K_\psi^L \psi^2 + K_\theta^L \left(\frac{\mathrm{d}w}{\mathrm{d}x}\right)^2\right)\right]_{x=0} + \left[\frac{1}{2}\left(K_t^R w^2 + K_\psi^R \psi^2 + K_\theta^R \left(\frac{\mathrm{d}w}{\mathrm{d}x}\right)^2\right)\right]_{x=L}. \tag{8}$$

The rotational spring reacts opposite to the moment forces as given in Eq.(4). Hence substituting equations (6) into equations (7) and (8) and simplifying gives

$$\begin{aligned}\Pi =& \frac{1}{2}\int_0^L \left(E\,I\left(\frac{68}{105}\left(\frac{\mathrm{d}\psi}{\mathrm{d}x}\right)^2 - \frac{32}{105}\frac{\mathrm{d}\psi}{\mathrm{d}x}\frac{\mathrm{d}^2 w}{\mathrm{d}x^2} + \frac{1}{21}\left(\frac{\mathrm{d}^2 w}{\mathrm{d}x^2}\right)^2\right) + \frac{8}{15}G\,A\left(\psi^2 + 2\,\psi\frac{\mathrm{d}w}{\mathrm{d}x} + \left(\frac{\mathrm{d}w}{\mathrm{d}x}\right)^2\right)\right) \\ &+ \left[\frac{1}{2}\left(K_t^L w^2 + K_\psi^L \psi^2 + K_\theta^L \left(\frac{\mathrm{d}w}{\mathrm{d}x}\right)^2\right)\right]_{x=0} + \left[\frac{1}{2}\left(K_t^R w^2 + K_\psi^R \psi^2 + K_\theta^R \left(\frac{\mathrm{d}w}{\mathrm{d}x}\right)^2\right)\right]_{x=L},\end{aligned} \tag{9}$$

where $I = \frac{W\,h^3}{12}$ is the cross-section moment of inertia, $\int\left(z^2, \frac{z^4}{h^2}, \frac{z^6}{h^4}\right)\mathrm{d}A = I\left(1, \frac{3}{20}, \frac{3}{112}\right)$ and $\int\left(1, \frac{z^2}{h^2}, \frac{z^4}{h^4}\right)\mathrm{d}A = A\left(1, \frac{1}{12}, \frac{1}{80}\right)$.

The velocities of any point on the beam are given by:

$$\begin{aligned}\dot{u} =& z\frac{\mathrm{d}\psi}{\mathrm{d}t} - \frac{4}{3h^2}z^3\left(\frac{\mathrm{d}\psi}{\mathrm{d}t} + \frac{\mathrm{d}^2 w}{\mathrm{d}x\,\mathrm{d}t}\right), \\ \dot{w} =& \frac{\mathrm{d}w}{\mathrm{d}t},\end{aligned} \tag{10}$$

and the average axial velocity is equal to zero i.e.

$$\dot{u}_{av} = \frac{\int_{-\frac{h}{2}}^{\frac{h}{2}} \dot{u}\,\mathrm{d}z}{h} = 0, \tag{11}$$

where $\int_{-\frac{h}{2}}^{\frac{h}{2}}\left(z, z^3\right)\mathrm{d}z = (0, 0)$.

The kinetic energy of the system T at any instant can be expressed as

$$\begin{aligned}T =& T_1 + T_2 = \frac{1}{2}\int_A\int_0^L \rho\left(\left(\frac{\mathrm{d}u}{\mathrm{d}t}\right)^2 + \left(\frac{\mathrm{d}w}{\mathrm{d}t}\right)^2\right)\mathrm{d}x\,\mathrm{d}A \\ &+ \left[\frac{1}{2}\left(m^L\left(\frac{\mathrm{d}w}{\mathrm{d}t}\right)^2\right)\right]_{x=0} + \left[\frac{1}{2}\left(m^R\left(\frac{\mathrm{d}w}{\mathrm{d}t}\right)^2\right)\right]_{x=L} \\ =& \frac{1}{2}\int_A\int_0^L \rho\left(\left(z^2\left(\frac{\mathrm{d}\psi}{\mathrm{d}t}\right)^2 - \frac{8}{3h^2}z^4\left(\left(\frac{\mathrm{d}\psi}{\mathrm{d}t}\right)^2 + \frac{\mathrm{d}\psi}{\mathrm{d}t}\frac{d^2 w}{\mathrm{d}x\,\mathrm{d}t}\right)\right.\right. \\ &\left.\left. + \frac{16}{9h^4}z^6\left(\frac{\mathrm{d}\psi}{\mathrm{d}t} + \frac{\mathrm{d}^2 w}{\mathrm{d}x\,\mathrm{d}t}\right)^2\right) + \left(\frac{\mathrm{d}w}{\mathrm{d}t}\right)^2\right)\mathrm{d}x\mathrm{d}A \\ &+ \left[\frac{1}{2}\left(m^L\left(\frac{\mathrm{d}w}{\mathrm{d}t}\right)^2\right)\right]_{x=0} + \left[\frac{1}{2}\left(m^R\left(\frac{\mathrm{d}w}{\mathrm{d}t}\right)^2\right)\right]_{x=L}\end{aligned} \tag{12}$$

where T_1 and T_2 refer to the kinetic energy of the beam and the attached masses respectively and ρ is the density of the beam material.

Simplifying Eq.(12) gives

$$T = \frac{1}{2}\int_0^L \left(\rho I\left(\frac{68}{105}\left(\frac{\mathrm{d}\psi}{\mathrm{d}t}\right)^2 - \frac{32}{105}\frac{\mathrm{d}\psi}{\mathrm{d}t}\frac{\mathrm{d}^2 w}{\mathrm{d}x\,\mathrm{d}t} + \frac{1}{21}\left(\frac{\mathrm{d}^2 w}{\mathrm{d}x\,\mathrm{d}t}\right)^2\right) + \rho A\left(\frac{\mathrm{d}w}{\mathrm{d}t}\right)^2\right)\mathrm{d}x + \left[\frac{1}{2}\left(m^L\left(\frac{\mathrm{d}w}{\mathrm{d}t}\right)^2\right)\right]_{x=0} + \left[\frac{1}{2}\left(m^R\left(\frac{\mathrm{d}w}{\mathrm{d}t}\right)^2\right)\right]_{x=L} \tag{13}$$

The work of the distributed transverse load $f(x,t)$ is given by

$$W = \int_0^L f w \mathrm{d}x. \tag{14}$$

Hamilton's principle can be used to obtain the equations of motion *i.e.*

$$\delta\int_{t_1}^{t_2}(\Pi - T - W)\mathrm{d}t = 0, \tag{15}$$

where the terms $\delta\int_{t_1}^{t_2}\Pi \mathrm{d}t$, $\delta\int_{t_1}^{t_2} T\mathrm{d}t$ and $\delta\int_{t_1}^{t_2} W\mathrm{d}t$ are given by:

$$\begin{aligned}\delta\int_{t_1}^{t_2}\Pi\mathrm{d}t = \int_{t_1}^{t_2}\int_0^L \Bigg[&EI\left(\frac{68}{105}\frac{\mathrm{d}\psi}{\mathrm{d}x}\,\delta\left(\frac{\mathrm{d}\psi}{\mathrm{d}x}\right) - \frac{16}{105}\frac{\mathrm{d}\psi}{\mathrm{d}x}\,\delta\left(\frac{\mathrm{d}^2 w}{\mathrm{d}x^2}\right) - \frac{16}{105}\frac{\mathrm{d}^2 w}{\mathrm{d}x^2}\,\delta\left(\frac{\mathrm{d}\psi}{\mathrm{d}x}\right) + \frac{1}{21}\frac{\mathrm{d}^2 w}{\mathrm{d}x^2}\delta\left(\frac{\mathrm{d}^2 w}{\mathrm{d}x^2}\right)\right)\\ &+ \frac{8}{15}GA\left(\psi\delta(\psi) + \psi\delta\left(\frac{\mathrm{d}w}{\mathrm{d}x}\right) + \frac{\mathrm{d}w}{\mathrm{d}x}\delta(\psi) + \frac{\mathrm{d}w}{\mathrm{d}x}\delta\left(\frac{\mathrm{d}w}{\mathrm{d}x}\right)\right)\Bigg]\mathrm{d}x\mathrm{d}t\\ &+ \int_{t_1}^{t_2}\Bigg[\left(K_t^L w\delta(w) + K_\psi^L\psi\delta(\psi) + K_\theta^L\frac{\mathrm{d}w}{\mathrm{d}x}\delta\left(\frac{\mathrm{d}w}{\mathrm{d}x}\right)\right)_{x=0}\\ &\left(K_t^R w\delta(w) + K_\psi^R\psi\delta(\psi) + K_\theta^R\frac{\mathrm{d}w}{\mathrm{d}x}\delta\left(\frac{\mathrm{d}w}{\mathrm{d}x}\right)\right)_{x=L}\Bigg]\mathrm{d}t\end{aligned} \tag{16}$$

$$\begin{aligned}\delta\int_{t_1}^{t_2} T_1\mathrm{d}t = \int_{t_1}^{t_2}\Bigg[\int_0^L \Bigg[&\rho I\left(-\frac{68}{105}\frac{\mathrm{d}^2\psi}{\mathrm{d}t^2}\,\delta(\psi) + \frac{16}{105}\frac{\mathrm{d}^2\psi}{\mathrm{d}t^2}\,\delta\left(\frac{\mathrm{d}w}{\mathrm{d}x}\right) + \frac{16}{105}\frac{\mathrm{d}^3 w}{\mathrm{d}x\mathrm{d}t^2}\,\delta(\psi) - \frac{1}{21}\frac{\mathrm{d}^3 w}{\mathrm{d}x\mathrm{d}t^2}\delta\left(\frac{\mathrm{d}w}{\mathrm{d}x}\right)\right)\\ &-\rho A\left(\frac{\mathrm{d}^2 w}{\mathrm{d}t^2}\delta(w)\right)\Bigg]\mathrm{d}x\Bigg]\mathrm{d}t + \int_{t_1}^{t_2}\left[\left(m^L\frac{\mathrm{d}^2 w}{\mathrm{d}t^2}\delta(w)\right)_{x=0} + \left(m^R\frac{d^2 w}{\mathrm{d}t^2}\delta(w)\right)_{x=L}\right]\mathrm{d}t,\end{aligned} \tag{17}$$

$$\delta\int_{t_1}^{t_2} W\mathrm{d}t = \int_{t_1}^{t_2}\left(\int_0^L f\delta(w)\,\mathrm{d}x\right)\mathrm{d}t. \tag{18}$$

Applying integration by parts to Eqs (16) and (17) gives

$$\begin{aligned}\delta\int_{t_1}^{t_2}\Pi \mathrm{d}t = \int_{t_1}^{t_2}\int_0^L \Bigg[& \left(-\frac{16}{105}EI\frac{\mathrm{d}^3\psi}{\mathrm{d}x^3}+\frac{1}{21}EI\frac{\mathrm{d}^4 w}{\mathrm{d}x^4}-\frac{8}{15}GA\left(\frac{\mathrm{d}\psi}{\mathrm{d}x}+\frac{\mathrm{d}^2 w}{\mathrm{d}x^2}\right)\right)\delta(w) \\ & +\left(-\frac{68}{105}EI\frac{\mathrm{d}^2\psi}{\mathrm{d}x^2}+\frac{16}{105}EI\frac{\mathrm{d}^3 w}{\mathrm{d}x^3}+\frac{8}{15}GA\left(\psi+\frac{\mathrm{d}w}{\mathrm{d}x}\right)\right)\delta(\psi)\Bigg]\mathrm{d}x\mathrm{d}t \\ & +\int_{t_1}^{t_2}\Bigg[\left(\frac{16}{105}EI\frac{\mathrm{d}^2\psi}{\mathrm{d}x^2}-\frac{1}{21}EI\frac{\mathrm{d}^3 w}{\mathrm{d}x^3}+\frac{8}{15}GA\left(\psi+\frac{\mathrm{d}w}{\mathrm{d}x}\right)\right)\delta(w)\Big|_0^L+\left[K_t^L w_0\delta(w0)+K_t^R w_L\delta(w_L)\right] \\ & +\left(-\frac{16}{105}EI\frac{\mathrm{d}\psi}{\mathrm{d}x}+\frac{1}{21}EI\frac{\mathrm{d}^2 w}{\mathrm{d}x^2}\right)\delta\left(\frac{\mathrm{d}w}{\mathrm{d}x}\right)\Big|_0^L+\left[K_\theta^L\frac{\mathrm{d}w_0}{\mathrm{d}x}\delta\left(\frac{\mathrm{d}w_0}{\mathrm{d}x}\right)+K_\theta^R\frac{\mathrm{d}w_L}{\mathrm{d}x}\delta\left(\frac{\mathrm{d}w_L}{\mathrm{d}x}\right)\right] \\ & +\left(\frac{68}{105}EI\frac{\mathrm{d}\psi}{\mathrm{d}x}-\frac{16}{105}\frac{\mathrm{d}^2 w}{\mathrm{d}x^2}\right)\delta(\psi)\Big|_0^L+\left(K_\psi^L\psi_0\delta(\psi_0)+K_\psi^R\psi_L\delta(\psi_L)\right)\Bigg]\mathrm{d}t\end{aligned} \tag{19}$$

$$\begin{aligned}\delta\int_{t_1}^{t_2}T\mathrm{d}t = \int_{t_1}^{t_2}\int_0^L \Bigg[& \left(-\frac{16}{105}\rho I\frac{\mathrm{d}^3\psi}{\mathrm{d}x\mathrm{d}t^2}+\frac{1}{21}\rho I\frac{\mathrm{d}^4 w}{\mathrm{d}x^2\mathrm{d}t^2}-\rho A\frac{\mathrm{d}^2 w}{\mathrm{d}t^2}\right)\delta(w) \\ & +\left(-\frac{68}{105}\rho I\frac{\mathrm{d}^2\psi}{\mathrm{d}t^2}+\frac{16}{105}\rho I\frac{\mathrm{d}^3 w}{\mathrm{d}x\mathrm{d}t^2}\right)\delta(\psi)\Bigg]\mathrm{d}x\,\mathrm{d}t \\ & +\int_{t_1}^{t_2}\left[\frac{16}{105}\rho I\,\frac{\mathrm{d}^2\psi}{\mathrm{d}t^2}-\frac{1}{21}\rho I\frac{\mathrm{d}^3 w}{\mathrm{d}x\mathrm{d}t^2}\right]_0^L\delta(w)\,\mathrm{d}t \\ & +\int_{t_1}^{t_2}\left[\left(-m^L\frac{\mathrm{d}^2 w_0}{\mathrm{d}t^2}\delta(w_0)\right)+\left(-m^R\frac{\mathrm{d}^2 w_L}{\mathrm{d}t^2}\delta(w_L)\right)\right]\mathrm{d}t\end{aligned} \tag{20}$$

Collecting the coefficients of $\delta(w)$ and $\delta(\psi)$ in Eqs (18-20) together gives the equations of motion:

$$\frac{16}{105}EI\frac{\mathrm{d}^3\psi}{\mathrm{d}x^3}-\frac{1}{21}EI\frac{\mathrm{d}^4 w}{\mathrm{d}x^4}+\frac{8}{15}GA\left(\frac{\mathrm{d}\psi}{\mathrm{d}x}+\frac{\mathrm{d}^2 w}{\mathrm{d}x^2}\right)+f=\frac{16}{105}\rho I\frac{\mathrm{d}^3\psi}{\mathrm{d}x\mathrm{d}t^2}-\frac{1}{21}\rho I\frac{\mathrm{d}^4 w}{\mathrm{d}x^2\mathrm{d}t^2}+\rho A\frac{\mathrm{d}^2 w}{\mathrm{d}t^2}, \tag{21}$$

$$-\frac{68}{105}EI\frac{\mathrm{d}^2\psi}{\mathrm{d}x^2}+\frac{16}{105}EI\frac{\mathrm{d}^3 w}{\mathrm{d}x^3}+\frac{8}{15}GA\left(\psi+\frac{\mathrm{d}w}{\mathrm{d}x}\right)=-\frac{68}{105}\rho I\frac{\mathrm{d}^2\psi}{\mathrm{d}t^2}+\frac{16}{105}\rho I\frac{\mathrm{d}^3 w}{\mathrm{d}x\mathrm{d}t^2}. \tag{22}$$

The boundary conditions for the Reddy beam are given in Table 1.

Table 1: Reddy beam boundary conditions.

Essential boundary conditions	Natural boundary conditions At left (x=0)	Natural boundary conditions At right (x=L)
w	$F_t = K_t^L w_0 + m^L\frac{\mathrm{d}^2 w_0}{\mathrm{d}t^2}$	$F_t = -K_t^R w_L - m^R\frac{\mathrm{d}^2 w_L}{\mathrm{d}t^2}$
$\frac{\mathrm{d}w}{\mathrm{d}x}$	$F_\theta = K_\theta^L\frac{\mathrm{d}w_0}{\mathrm{d}x}$	$F_\theta = -K_\theta^R\frac{\mathrm{d}w_L}{\mathrm{d}x}$
ψ	$F_\psi = K_\psi^L\psi_0$	$F_\psi = -K_\psi^R\psi_L$

where $F_t = \frac{16}{105}EI\frac{\mathrm{d}^2\psi}{\mathrm{d}x^2}-\frac{1}{21}EI\frac{\mathrm{d}^3 w}{\mathrm{d}x^3}+\frac{8}{15}GA\left(\psi+\frac{\mathrm{d}w}{\mathrm{d}x}\right)-\frac{16}{105}\rho I\frac{\mathrm{d}^2\psi}{\mathrm{d}t^2}-\frac{1}{21}\rho I\frac{\mathrm{d}^3 w}{\mathrm{d}x\mathrm{d}t^2}$,
$F_\theta = -\frac{16}{105}EI\frac{\mathrm{d}\psi}{\mathrm{d}x}+\frac{1}{21}EI\frac{\mathrm{d}^2 w}{\mathrm{d}x^2}$ and $F_\psi = \frac{68}{105}EI\frac{\mathrm{d}\psi}{\mathrm{d}x}-\frac{16}{105}EI\frac{\mathrm{d}^2 w}{\mathrm{d}x^2}$.

2.2. Element mass and stiffness matrices of Reddy beam

The beam was divided into J elements and $N = J + 1$ nodes. Each j^{th} element has 2 nodes as shown in Fig.3-(a). Equations (16-18) show that the transverse displacement w and the rotation ψ are required to be at least twice and

once differentiable, respectively. In order to obtain the element mass and stiffness matrices, exact integration is used with linear Lagrange $\mathbf{L_i}$ and Hermite cubic $\mathbf{H_i}$ interpolation functions for ψ and w:

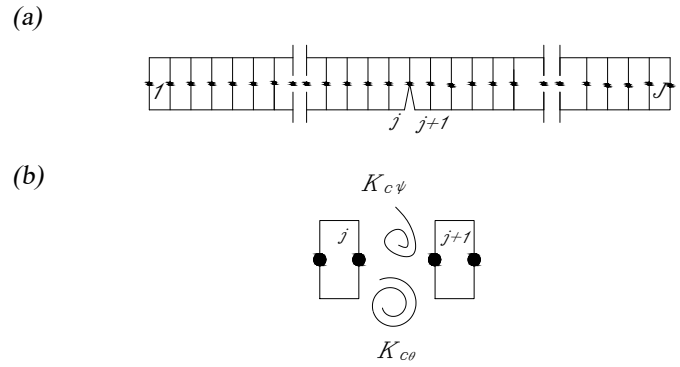

Figure 3: Schematic diagrams of (a) the Reddy beam finite element model (b) the crack rotational spring model

$$\psi(x,t) = \sum_{i=1}^{2} \psi_i(t)\ L_i(x) \text{ and } w(x,t) = \sum_{i}^{4} \Delta_i(t)\ H_i(x), \tag{23}$$

whereΔ_i is as given by:

$$\begin{aligned} &\Delta_1 = [w]_{x=x_j},\ \Delta_2 = [\theta]_{x=x_j} = \left[-\frac{\mathrm{d}w}{\mathrm{d}x}\right]_{x=x_j}, \\ &\Delta_3 = [w]_{x=x_{j+1}} \text{ and } \Delta_4 = [\theta]_{x=x_{j+1}} = \left[-\frac{\mathrm{d}w}{\mathrm{d}x}\right]_{x=x_{j+1}}, \end{aligned} \tag{24}$$

and (x_j, x_{j+1}) are the global nodal coordinates of the j^{th} element. Substituting Eq (23) into Eqs (16-18) gives the element equation. The Reddy beam has 6×6 stiffness $\mathbf{K_e}$ and mass $\mathbf{M_e}$ matrices with nodal-value vector $\mathbf{\Delta_e} = [\Delta_1 \Delta_2 \psi_1 \Delta_3 \Delta_4 \psi_2]$ and force vector $\mathbf{F_e}$

$$\left(\mathbf{K}_e - \omega^2 \mathbf{M}_e\right) \mathbf{\Delta}_e = \mathbf{F_e} \tag{25}$$

These matrices are given in Appendix A.

The transverse and rotational elastic support at the j^{th} node is given by a diagonal 3×3 matrix;

$$\mathbf{K_{s_j}} = \begin{bmatrix} K_{w_j} & 0 & 0 \\ 0 & K_{\theta_j} & 0 \\ 0 & 0 & K_{\psi_j} \end{bmatrix} \tag{26}$$

2.3. Crack model

In several studies, the crack is modeled as a massless rotational spring, whose stiffness can be calculated using fracture mechanics which leads to a substructure approach (Aria et al., 2019; Banerjee and Guo, 2009; Kisa et al., 1998; Labib et al., 2014; Loya et al., 2009; Mazaheri et al., 2018; Torabi and Nafar Dastgerdi, 2012). Consider the cracked node to be a cracked element with no length and no mass. The key benefit of this approach is that the global nonlinear structure is divided into multiple linear subsystems with a local stiffness discontinuity. In the

present analysis, the lateral stiffness of the beam at the crack position is assumed to have remained unchanged and the continuity conditions at the crack location imply that the vertical deflections at the left and right nodes are identical. The total equivalent stiffness for crack rotary spring is assumed to be related to the crack depth a by:

$$K^{eq} = \frac{E\,I}{L}\frac{1}{k^*} \text{ where } k^* = \frac{h}{L}\,C(\xi), \tag{27}$$

where k^* is a dimensionless local compliance which is a measure of crack severity, $C(\xi)$ is a dimensionless function given by (Caddemi and Caliò, 2009, 2013):

$$C(\xi) = \frac{\xi\ (2-\xi)}{0.9\ (\xi-1)^2}\,. \tag{28}$$

and $\xi = \frac{a}{h}$ is the crack depth to height ratio. The stiffness of the equivalent rotational spring K^{eq} in the cracked node position was determined by Eq (27). In the case of uncracked nodes, the value of K^{eq} approaches infinity.

In the Reddy beam the beam cross sections are pinned together by 2 parallel rotary springs as shown in Fig.3-(b) which are used to model the increased flexibility due to the crack, where the subscript c means crack. $(\psi^L,\ \theta^L)$ and $\left(\psi^R, \theta^R\right)$ are the rotation and bending slope at left and right ends of the element, respectively; w is the lateral displacement of the node; and K_ψ and K_θ are the components of rotational stiffness corresponding to ψ and θ respectively. Based on Eq (4), $K_{c\psi}$ and $K_{c\theta}$ can be expressed as $\frac{2}{3}K^{eq}$ and $\frac{1}{3}K^{eq}$ respectively. The continuity conditions at the crack location demonstrate that the left and right nodes have the same vertical deflection $w^L = w^R$; *i.e.*, the node connecting stiffness is infinity in this direction. However, the rotations ψ^L, θ^L and $\psi^R,\ \theta^R$ of these nodes are related through the torsional stiffness. The stiffness matrix of the crack can be written as:

$$\mathbf{K_c} = \begin{bmatrix} \infty & 0 & 0 & -\infty & 0 & 0 \\ 0 & K_{c\theta} & 0 & 0 & -K_{c\theta} & 0 \\ 0 & 0 & K_{c\psi} & 0 & 0 & -K_{c\psi} \\ -\infty & 0 & 0 & \infty & 0 & 0 \\ 0 & -K_{c\theta} & 0 & 0 & K_{c\theta} & 0 \\ 0 & 0 & -K_{c\psi} & 0 & 0 & K_{c\psi} \end{bmatrix} \tag{29}$$

2.4. Global stiffness and mass matrix

In this global matrix, there are N nodes and n cracks leading to a $3(N+n) \times 3(N+n)$ matrix. The assembly technique for the cracked beam follows the traditional finite element technique. The overall stiffness $\mathbf{K}$ and mass $\mathbf{M}$ matrices of a cracked Reddy beam can be assembled as shown in Fig.4.

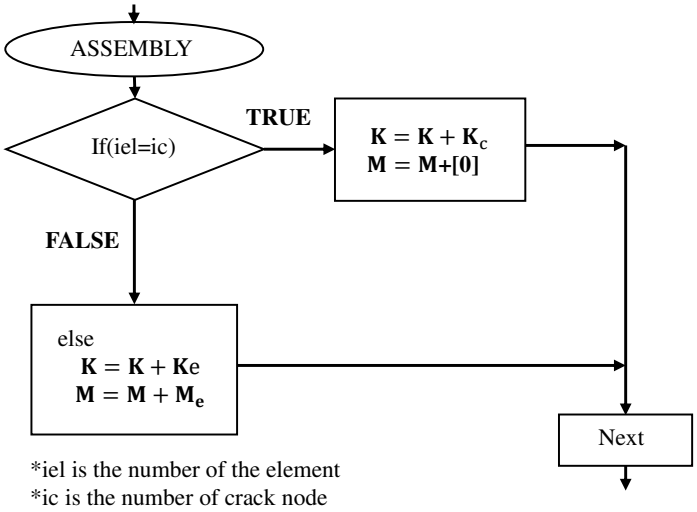

Figure 4: Finite element assembly technique.

2.5. Determination of natural frequencies and mode shapes

The natural frequencies and mode shapes of an undamped beam in free vibration analysis can be obtained using global stiffness **K** and mass **M** matrices. In general, the undamped eigenvalues can be obtained using

$$\left[\mathbf{K} - \omega_i^2 \mathbf{M}\right] \mathbf{d} = 0, \tag{30}$$

where, ω_i is the natural frequency and **d** is the mode shape vector of the beam. MATLAB code was used to obtain the natural frequencies and the mode shapes of the beam.

2.6. Finite element model using ANSYS

To validate the results of the present model, selected cases were solved using the present finite element model based on Reddy beam theory and using real cracked beam geometry model using the ANSYS finite element package (El-Sayed and Hand, 2011). The cracked beams were modeled in three-dimensions using SOLID186 elements. A mapped mesh was used for the selected model as shown in Fig.5. The number of elements used to mesh the model was 20000. The boundary conditions were identified according to the investigated case as clamped, simply supported, or free. The analysis was performed using ANSYS Modal module.

2.7. Experimental setup

To investigate the accuracy of the present model in a practical application, selected samples were prepared and experimentally tested. These samples were manufactured from steel. The length of the samples was $L = 0.3$ m and the width and height of the samples were $W = h = 0.02$ m . The density of the material was experimentally evaluated as 7800±16 kg/m^3. The elastic modulus of the material was evaluated based on the free vibration analysis of an uncracked beam as 202±3 GPa.

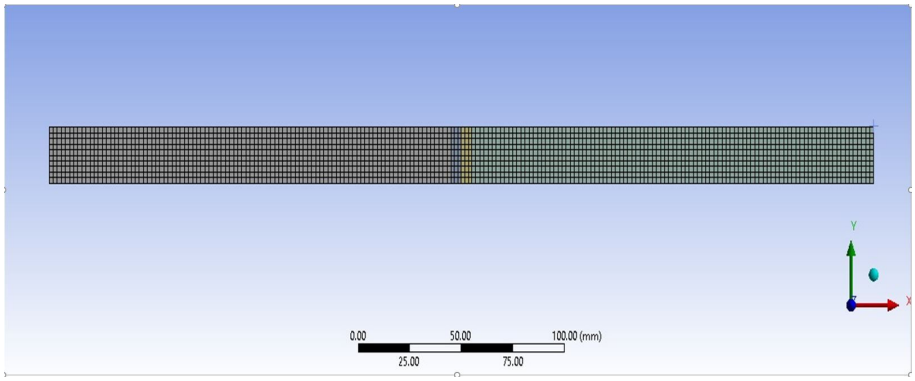

Figure 5: ANSYS model of cracked beam.

The experimental setup as based on the free vibration of cracked and uncracked samples. The beam was excited using instrumented hammer model B&K 8202. A low weight accelerometer model B&K 4375 was used, to reduce the effect of accelerometer mass on the results. This accelerometer was connected to a charge amplifier Model B&K 2635. The analog output from this amplifier was connected to a NI data acquisition card (model NI6216), see Fig.6-b, which was directly connected to a laptop. LABVIEW software was used to capture the results in real-time. The signal capture settings were a sample frequency of 8 kHz, sampling time 5 s with a 2 k sample block. The obtained experimental frequency was calculated based on the average of at least 6 measurements for each single case. For each case the measurements were performed using at least two locations for the accelerometer to avoid coinciding the accelerometer location with a standing wave node which would have resulted in the mode being missed. This was found to help to capture all the first vibration modes more precisely. Several crack locations and crack depths were used in the present analysis; the cracked samples are shown in Fig.6-b. The dimensions and location of the crack are listed in Table 2. Four different crack depth ratios namely $\xi = 0,\ 0.2,\ 0.4,\ 0.6$ were used.

Table 2: The dimensions and crack location ratios of the five samples.

Samples	L (m)	W (m)	h (m)	l_c
S_1				0.1
S_2				0.2
S_3	0.3	0.02	0.02	0.3
S_4				0.4
S_5				0.5

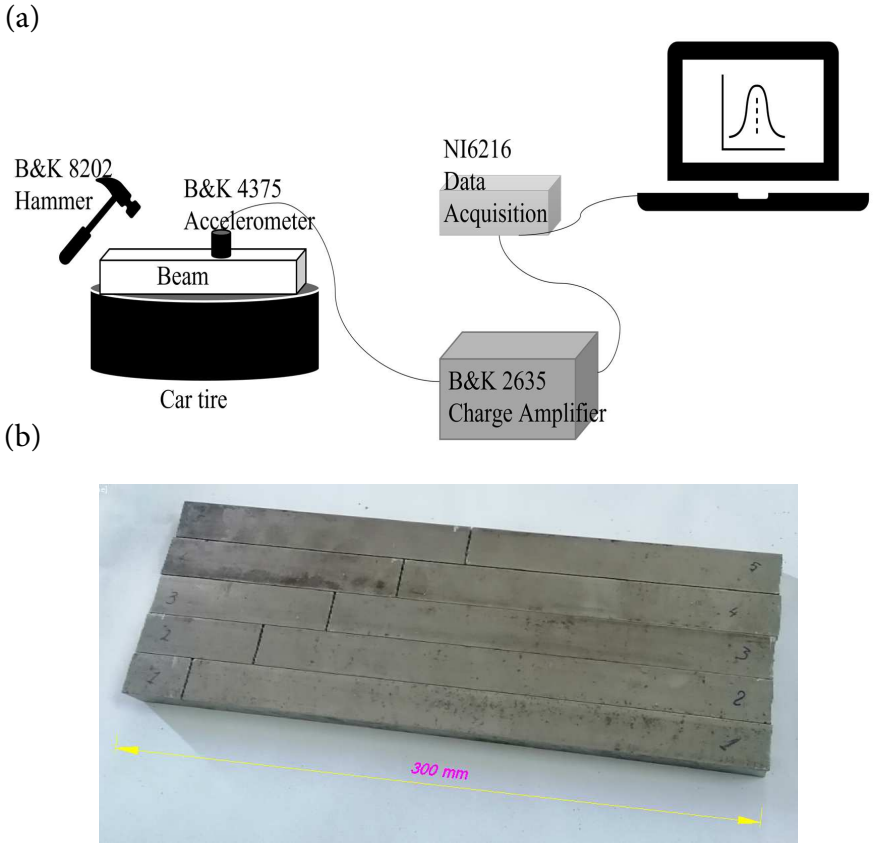

Figure 6: (a) Experimental setup (b)Cracked steel test samples

3. Results and discussion

This section is divided into two subsections. In the first subsection validation results for the present model are compared with some published literature. In the second subsection, new results are presented and discussed. The following dimensionless parameters are employed throughout the present work, $\bar{\omega} = \left(\frac{\rho A}{E I}\omega^2 L^4\right)^{\frac{1}{4}}$, $\Omega = \frac{\omega_{cr}}{\omega_{int}}$, $\xi = \frac{a}{h}$, $l_c = \frac{L_c}{L}$,

where $\bar{\omega}$, $\omega_{cr}, \omega_{int}, \Omega$, ξ, l_c are respectively the dimensionless frequency, the frequency of the cracked beam, the frequency of the intact beam, the frequency ratio, the crack depth ratio and the crack position ratio. $\hat{\omega} = \frac{\omega}{2\pi}$ is the frequency in Hertz.

3.1. Validation of the present cracked Reddy beam model

The effects of aspect ratio and crack (depth and position) on the beam frequencies were independently investigated and compared with the literature in order to present a comprehensive verification procedure. Initially, the results were obtained for an intact beam with various aspect ratios as shown in Table 3. Then, the natural frequencies for a cracked beam with varying crack depths and positions were calculated and are compared in Table 4.

The first six dimensionless natural frequencies $\bar{\omega}_n$ for an intact clamped-simply supported beam are compared with those from Ref. (Şimeşk and Kocatürk, 2007) as shown in Table 3. The analysis was applied for different aspect ratios $\frac{h}{L} = 0.002,\ 0.01,\ 0.02,\ 0.05,\ 0.1,\ 0.2$.

The results of the present model, 3D-FE and those based on FSDT (Torabi and Nafar Dastgerdi, 2012) and ones based on CBT (Aria et al., 2019; Loya et al., 2009) were compared. A slenderness ratio of 0.1 is considered in the present TSDT and 3D-FE results. The effect of crack position ratio ($l_c = 0.5,\ 0.25$) and crack severity parameter ($k^* = 0.065,\ \ 0.35,\ 2$) or crack depth ratio ($\xi = 0.028,\ 0.128,\ 0.402$) were examined. For further validation, the results for simply supported-simply supported boundary conditions are given in Table 4. In this comparison first four dimensionless natural frequencies are compared.

This concludes the procedure for detailed examination of the current model. There is good agreement between the results of this analysis, the 3D-FE results and literature data.

Table 3: The first six dimensionless natural frequency $\bar{\omega}_n$ of an intact clamped-simply supported beam for different aspect ratios $\frac{h}{L}$

Method	$\frac{h}{L}$	$\bar{\omega}_1$	$\bar{\omega}_2$	$\bar{\omega}_3$	$\bar{\omega}_4$	$\bar{\omega}_5$	$\bar{\omega}_6$
a	0.002	3.9265	7.0684	10.2097	13.3508	16.4916	19.6322
present		3.9266	7.0685	10.2099	13.3511	16.4921	19.6328
a	0.005	3.9264	7.0676	10.2074	13.3459	16.4826	19.6173
present		3.9264	7.0676	10.2075	13.3460	16.4828	19.6174
a	0.01	3.9258	7.0647	10.1992	13.3284	16.4506	19.5646
present		3.9258	7.0647	10.1993	13.3285	16.4507	19.5644
a	0.02	3.9234	7.0531	10.1671	13.26	16.3266	19.3624
present		3.9235	7.0531	10.1671	13.2600	16.3264	19.3616
a	0.05	3.9072	6.9754	9.9582	12.8349	15.5932	18.2290
present		3.9073	6.9754	9.9582	12.8349	15.5930	18.2281
a	0.1	3.8525	6.7346	9.3769	11.7802	13.9692	15.9742
present		3.8526	6.7350	9.3778	11.7819	13.9716	15.9774
a	0.2	3.6708	6.0947	8.1219	9.8636	11.3979	12.7717
present		3.6710	6.0957	8.1237	9.8662	11.4010	12.7753

(a) refers to Şimşek and Kocatürk (Şimeşk and Kocatürk, 2007) results.

3.2. Vibration of a cracked Reddy beam

3.2.1. Crack depth and location effect on the beam natural frequency using TSDT, FSDT, CBT and 3D-FE.

The number of elements used in the MATLAB code for TSDT is 100 elements. The changes in the first frequency $\hat{\omega}_1$ of a cracked beam for crack depth ratios ($\xi = 0,\ 0.2,\ 0.4,\ 0.6$) and different boundary conditions versus crack location ratios l_c are presented in Fig.7. Figure 7 also compares the TSDT , FSDT and CBT with FE results for thick and thin beams with slenderness ratios ($\lambda = 20,\ \ 40$) and beam lengths $L = 0.4\ ,\ 0.8$ m respectively.

There is good agreement between TSDT, FSDT, CBT, and the FE results for the frequency of the first vibrational mode. As the crack depth ratio increases, the first frequency decreases, indicating a reduction in the stiffness of the cracked beams for both thin and thick beams and for the different boundary conditions. For the same crack depth and

Table 4: The first four dimensionless natural frequencies $\bar{\omega}_{\mathbf{n}}$ of a cracked simply supported-simply supported beam for different crack position ratios $\mathbf{l_c}$ and crack severity $\mathbf{k}^*$.

k^*	ξ	$\bar{\omega}_n$	l_c	Present	3D-FE	a	b	c	l_c	Present	3D-FE	a	b	c
0.065	0.2057	$n=1$	0.5	3.0186	3.0601	3.0469	2.9379	3.0466	0.25	3.0650	3.0846	3.0921	3.024	3.0925
		$n=2$		6.0930	6.0974	6.2832	6.1583	6.2818		5.9228	5.9855	6.1028	5.8101	6.1019
		$n=3$		8.6316	8.7224	9.1669	8.5536	9.1652		8.7450	8.7879	9.3021	8.8166	9.3005
		$n=4$		11.3578	11.3816	12.5664	11.717	12.5638		11.3578	11.3815	12.5664	11.717	12.5642
0.35	0.5091	$n=1$		2.7238	2.7214	2.7496	2.3533	2.7489		2.8809	2.8790	2.9071	2.596	2.9064
		$n=2$		6.0930	6.0900	6.2832	6.1583	6.2819		5.5041	5.4887	5.6491	4.9441	5.6484
		$n=3$		8.1679	8.3652	8.6129	7.3535	8.6114		8.5576	8.5040	9.0767	8.4026	9.0752
		$n=4$		11.3578	11.3104	12.5664	11.717	12.5638		11.3578	11.3395	12.5664	11.717	12.5642
2	0.7706	$n=1$		2.0843	2.1788	2.096	1.3055	2.0958		2.3345	2.2948	2.3493	1.5023	2.3465
		$n=2$		6.0930	6.0654	6.2832	6.1583	6.2818		4.9976	5.2813	5.1047	4.3015	5.1042
		$n=3$		7.7000	8.1824	8.073	6.3928	8.0715		8.4064	8.1396	8.9008	8.1377	8.8993
		$n=4$		11.3578	11.1176	12.5664	11.717	12.5638		11.3578	11.1941	12.5664	11.717	12.5642
Intact beam		$n=1$		3.1160	3.1167	3.1416	3.1252	3.1409						
		$n=2$		6.0930	6.0977	6.2832	6.1583	6.2818						
		$n=3$		8.8475	8.8606	9.4248	9.0328	9.4228						
		$n=4$		11.3578	11.3828	12.5664	11.717	12.5638						

(a)Loya et al. (2009), (b) Torabi and Nafar Dastgerdi (2012), (c) Aria et al. (2019) and n is the mode index.

location ratios, the vibration frequency of a thick (short) beam decreased more than that of a thin (long) beam, indicating that the vibrations of thick (short) beams are more sensitive to the presence of cracks. Each boundary condition has a crack location where the crack depth has a negligible effect on the frequency and the behavior resembles that of the intact beam; these locations are referred to as blind locations. There are also some locations where the influence of crack depth on frequency is maximised; these are referred to as sensitive locations.

The first three natural frequencies of the cracked beam with a slenderness ratio $\lambda = 20$, length $L = 0.4$ m and crack depth ratio $\xi = 0.4$ with respect to crack location ratio l_c are shown in Fig. 8. The results of Fig. 8 show clearly that the results of both TSDT, FSDT are very close together in all modes and for all boundary conditions. In addition, it can be shown from the same figure that CBT results are closer to 3D-FE results at the first mode while TSDT, FSDT results are closer to the 3D-FE results for the 2nd and 3rd modes. As shown in Fig. 8, the blind and sensitive locations for every boundary condition change with changing the vibration mode. The change in blind and sensitive locations ratios as extracted from Fig. 7 and Fig. 8 are tabulated in Table 5 for different boundary conditions and for the first three modes.

3.2.2. Crack depth and location effect using TSDT, FSDT, CBT, experimental and 3D-FE

Here, the samples discussed in experimental setup section are used. There are five samples with crack location ratios [0.1, 0.2, 0.3, 0.4, 0.5] for $[S_1, S_2, S_3, S_4, S_5]$ respectively. The number of elements used in the TSDT method is 400 elements. The test samples are supported on a flexible car tire inner tube to simulate the free-free end conditions.

The changes in the first three natural frequencies $\hat{\omega}_n$ of the cracked beam versus crack depth ratios ($\xi = 0,\ 0.2,\ 0.4,\ 0.6$) for different crack location ratios l_c and for free-free boundary conditions are compared with the TSDT, FSDT, CBT and 3D-FE results in Fig.9. The percentage deviations between the model results and the experimental results are listed in Table 6.

Table 5: The blind and sensitive locations ratios for first three modes and different boundary conditions.

Mode number	Blind locations ratios	Sensitive locations ratios
	C-C	
$n = 1$	0.25 and 0.75	Clamped ends and mid-point
$n = 2$	0.15, 0.5 and 0.85	0.3, 0.7 and clamped ends
$n = 3$	0.1, .35, 0.65 and 0.9	0.2, 0.8, Clamped ends and mid-point
	S-S	
$n = 1$	simply supported ends	Mid-point
$n = 2$	Mid-point and simply supported ends	0.25 and 0.75
$n = 3$	0.35, 0.65 and simply supported ends	0.15, 0.85 and mid-point
	C-S	
$n = 1$	0.25 and simply supported end	0.65 and clamped end
$n = 2$	0.15, 0.55 and simply supported end	0.35, 0.8 and clamped end
$n = 3$	0.1, 0.4, 0.7 and simply supported end	0.25, 0.55, 0.85 and clamped end
	C-F	
$n = 1$	Free end	Clamped end
$n = 2$	0.2 and free end	0.55 and clamped end
$n = 3$	0.15, 0.5 and free end	0.3, 0.7 and clamped end

The results shown in Fig.9 and Table 6 indicate better agreement between the experimental results and TSDT, FSDT and 3D-FE than CBT, especially for higher modes. Figures 7-9, and Table 6 show that the results of FSDT are very close to the TSDT. It is worth noting that the FSDT and TSDT results are very close together, however, the FSDT model has an advantage over the TSDT model in that it does not require the evaluation of a shear correction coefficient κ. The calculated maximum deviation between the present TSDT analysis and the experimental results is less than 3.07 %. However, the maximum deviation between 3D-FE results and the experimental results is less than 1.73%. This means that the 3D-FE gives a more accurate prediction of the experimental results than TSDT. However, TSDT has the advantage of being a line element model with less elements and thus lower memory requirements for its solution.

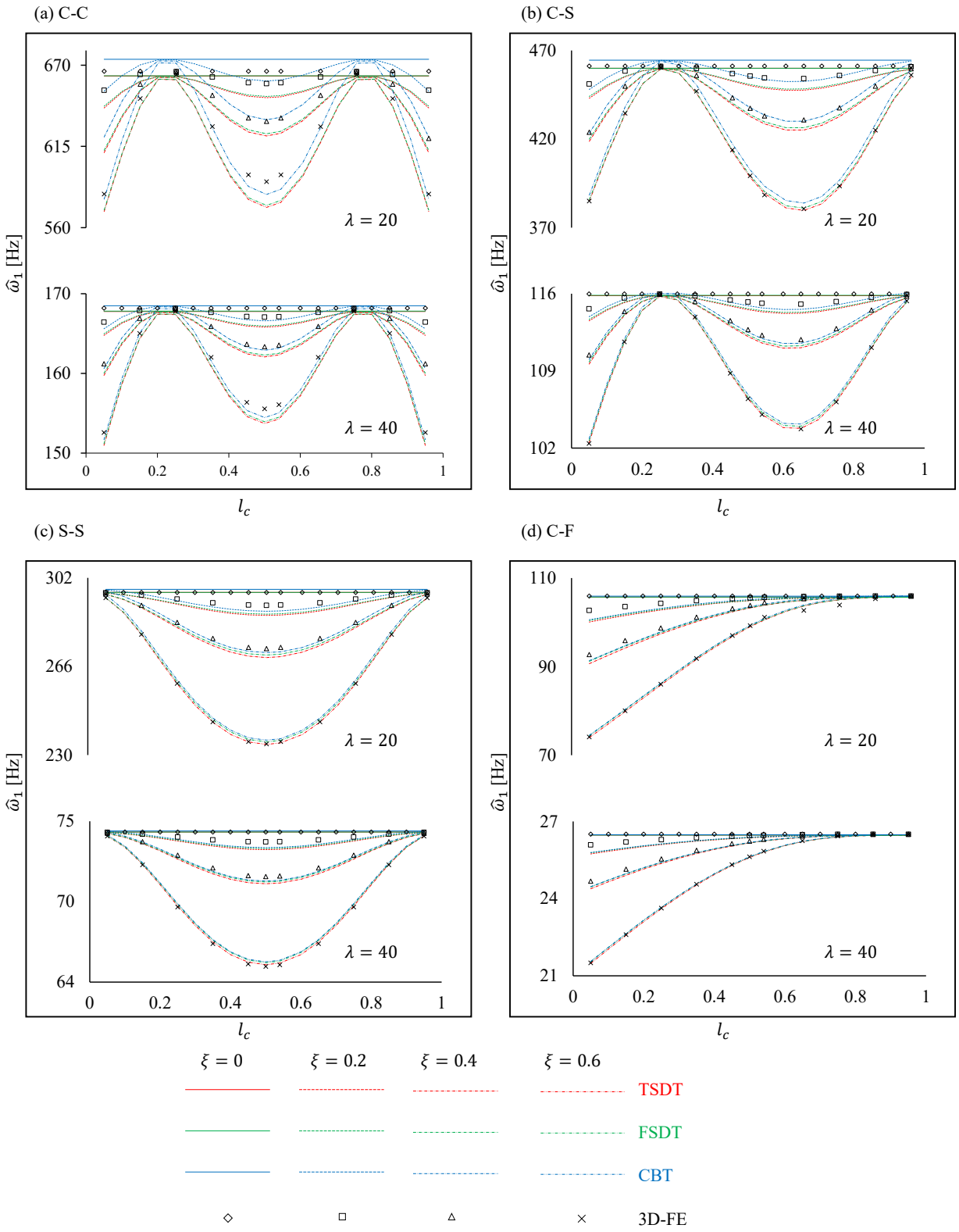

Figure 7: First natural frequency of cracked beam versus crack location ratio l_c for different crack depths

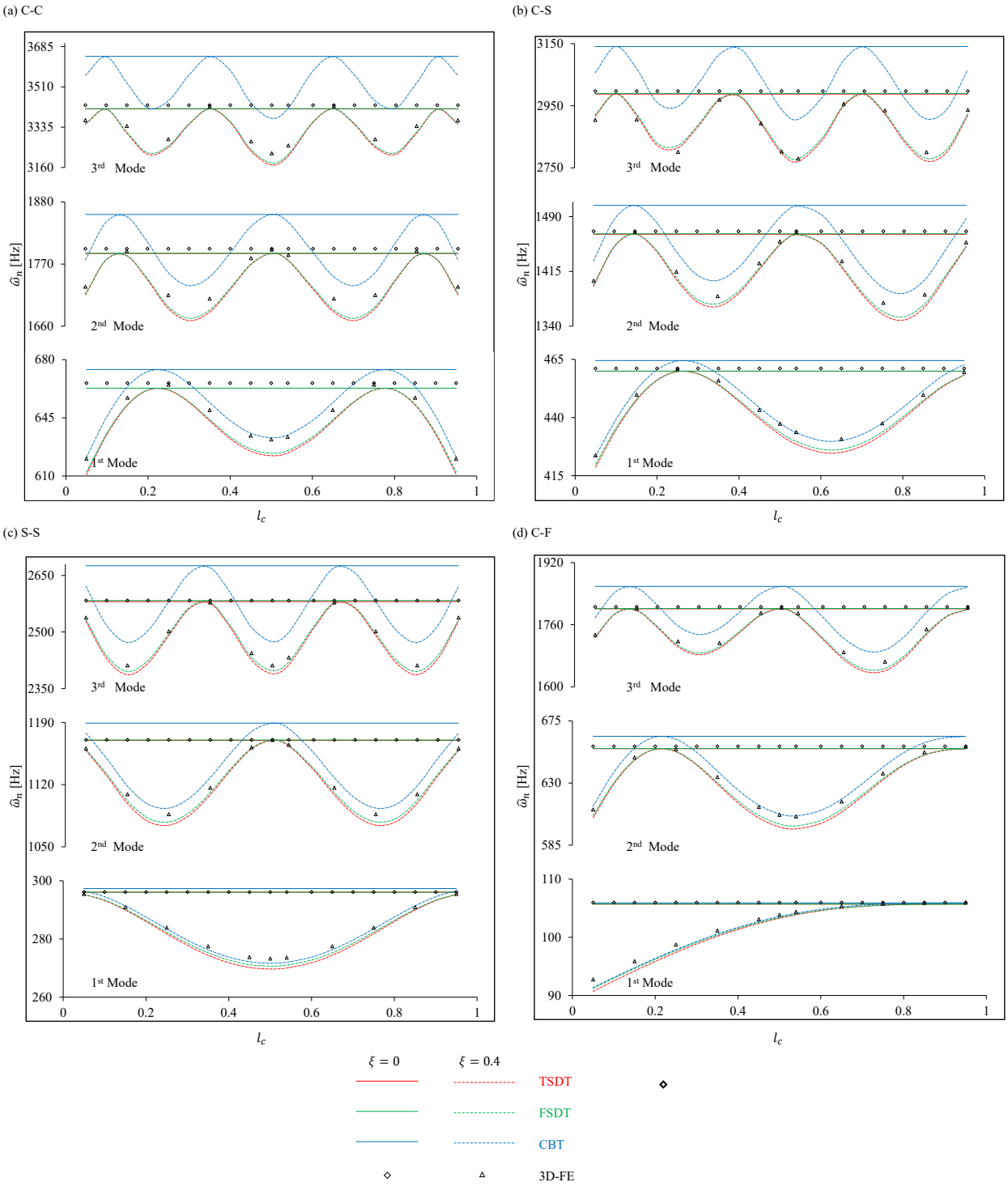

Figure 8: First three natural frequency of cracked beam versus crack location ratio.

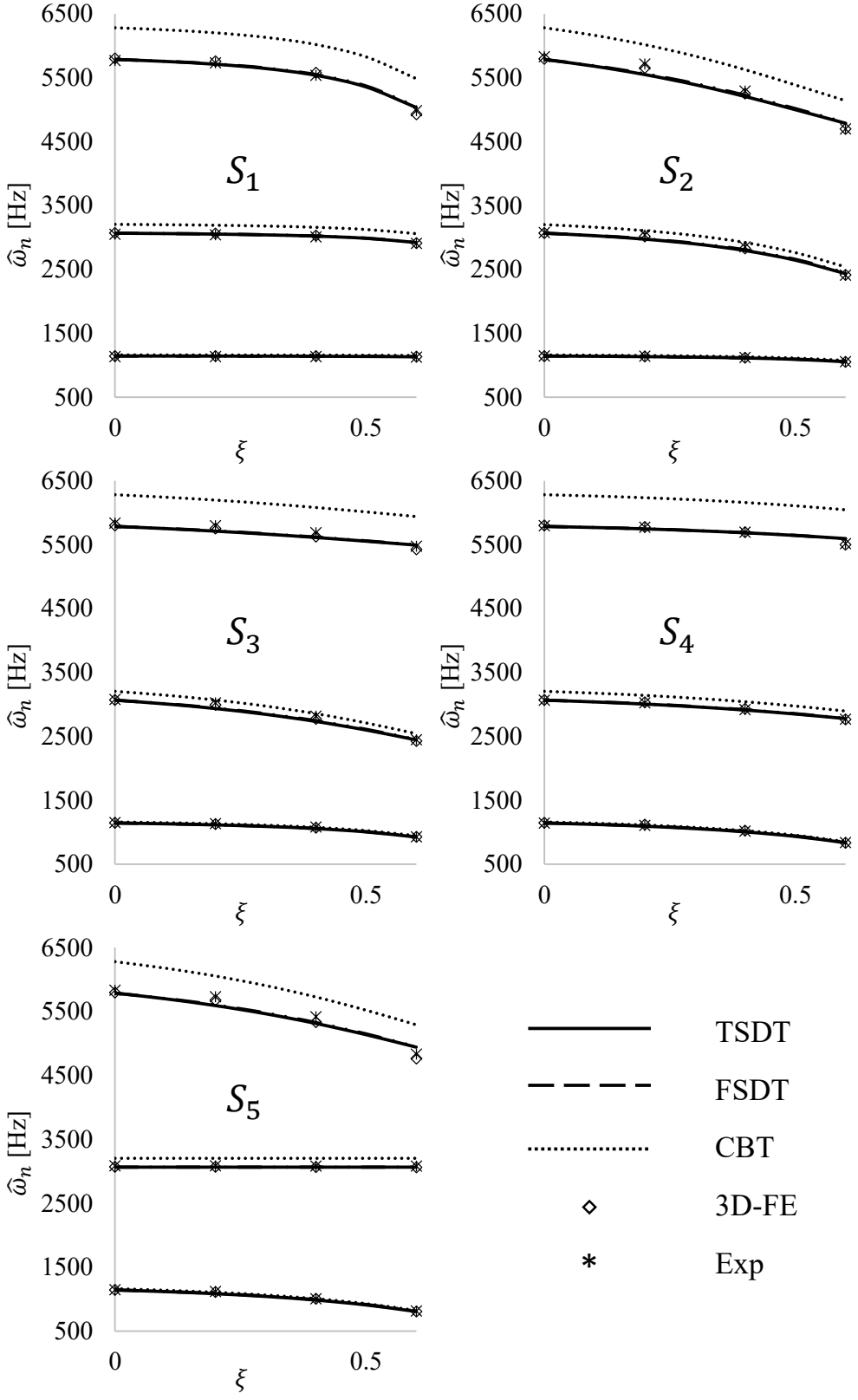

Figure 9: First three natural frequency of cracked beam versus crack depth ratio.

Table 6: The deviation of the TSDT and 3D-FE results from the experimental results.

	ξ	Method	n_1	n_2	n_3		ξ	Method	n_1	n_2	n_3
	0	TDST	0.76	0.61	0.35		0	TDST	-0.4	-0.42	-0.76
		FSDT	0.77	0.61	0.35			FSDT	-0.4	-0.42	-0.76
		CBT	2.33	4.89	8.19			CBT	1.18	3.90	7.17
		3D-FE	0.8	0.71	0.55			3D-FE	-0.37	-0.32	-0.55
	0.2	TDST	0.67	0.32	-0.33		0.2	TDST	-0.9	-2.34	-2.96
		FSDT	0.68	0.36	-0.24			FSDT	-0.84	-2.15	-2.72
		CBT	2.24	4.65	7.60			CBT	0.74	2.14	5.02
S_1		3D-FE	0.74	0.64	0.46	S_2		3D-FE	-0.48	-0.87	-1.03
	0.4	TDST	0.57	0.4	0.05		0.4	TDST	-1.03	-2.14	-1.64
		FSDT	0.58	0.47	0.28			FSDT	-0.9	-1.72	-1.29
		CBT	2.16	4.77	8.03			CBT	0.68	2.35	5.92
		3D-FE	0.63	0.7	0.76			3D-FE	-0.6	-0.82	-0.75
	0.6	TDST	0.58	0.48	1.02		0.6	TDST	-0.12	0.99	1.85
		FSDT	0.6	0.63	1.4			FSDT	0.11	1.45	2.05
		CBT	2.19	5.03	9.17			CBT	1.69	5.10	8.61
		3D-FE	0.58	0.23	-1.14			3D-FE	-0.18	0.15	0.06

	ξ	Method	n_1	n_2	n_3		ξ	Method	n_1	n_2	n_3
	0	TDST	-0.52	-0.33	-0.81		0	TDST	0.25	0.02	-0.13
		FSDT	-0.52	-0.33	-0.81			FSDT	0.25	0.03	-0.13
		CBT	1.07	3.99	7.12			CBT	1.82	4.33	7.75
		3D-FE	-0.48	-0.23	-0.61			3D-FE	0.28	0.13	0.07
	0.2	TDST	-1.88	-2.98	-1.48		0.2	TDST	-1.17	-0.63	-0.42
		FSDT	-1.72	-2.72	-1.41			FSDT	-0.90	-0.52	-0.38
		CBT	-0.14	1.49	6.46			CBT	0.63	3.71	7.43
S_3		3D-FE	-0.68	-1.02	-0.77	S_4		3D-FE	0.8	0.3	0.06
	0.4	TDST	-2.46	-3.07	-1.3		0.4	TDST	-0.93	-0.24	-0.16
		FSDT	-2.09	-2.64	-1.2			FSDT	-0.38	-0.06	-0.10
		CBT	-0.56	1.27	6.53			CBT	1.04	4.00	7.55
		3D-FE	-1.27	-1.73	-1.07			3D-FE	0.86	0.34	-0.02
	0.6	TDST	-0.16	-0.08	0.33		0.6	TDST	-0.11	0.5	1.4
		FSDT	0.35	0.23	0.38			FSDT	0.54	0.63	1.44
		CBT	1.76	3.67	7.87			CBT	1.79	4.47	8.80
		3D-FE	-0.27	-0.85	-0.9			3D-FE	-0.22	-0.04	-0.26

	ξ	Method	n_1	n_2	n_3
	0	TDST	-0.4	-0.67	-0.8
		FSDT	-0.4	-0.67	-0.8
		CBT	1.18	3.67	7.13
		3D-FE	-0.37	-0.56	-0.59
	0.2	TDST	-3.05	-0.67	-2.52
		FSDT	-2.73	-0.67	-2.33
		CBT	-1.19	3.66	5.33
S_5		3D-FE	-0.72	-0.57	-0.95
	0.4	TDST	-2.19	-0.63	-2
		FSDT	-1.56	-0.63	-1.72
		CBT	-0.16	3.71	5.38
		3D-FE	-0.16	-0.57	-1.62
	0.6	TDST	-1.2	-0.5	2.23
		FSDT	-0.49	-0.5	2.41
		CBT	0.72	3.83	8.66
		3D-FE	-1.31	-0.61	-1.45

Conclusion

This paper aims to obtain the natural frequencies of cracked Reddy beams using the finite element method. The cracked beam was solved by assembling the intact beams elements together with crack elements located at the appropriate crack location. Two rotational springs with stiffnesses dependent on crack depth were used for the crack element. The study examines the effect of boundary conditions, slenderness ratio, crack location and crack depth on the frequencies.

From the obtained results, the following conclusions can be drawn:

• The cracked beam natural frequency decreases due to the loss of the equivalent beam flexibility. The amount of decrease is determined by the crack depth, and crack location.

• For the same crack location and depth ratio, the percentage reduction of the natural frequency for the thick (short) beam is greater than for thin (long) beams.

• The cracked beam has blind and sensitive locations that change by changing the boundary conditions and the mode of vibration. The impact of a crack is more obvious at the fixed end than the free end. The blind locations differ from the nodes of mode shapes.

• The CBT analysis is accurate for evaluating the first vibrational mode but not for evaluating higher modes.

• The results of both TSDT and FSDT are very close together and they prove an excellent agreement with the experimental results and the 3D-FE models, especially for higher modes. However, it is important to highlight that the advantage of TSDT over FSDT is that it does not require the evaluation of a shear correction coefficient κ..

• The effects of cracks on the higher-order frequencies tend to be clearer.

• To detect the crack on the beam it is important to check a lot of modes or boundary conditions for the beam.

The suggested approach is not restricted to the topics discussed in this study; it may also be applied to cracked beams with numerous cracks. It should be emphasized that damping is not considered in this study. As a result, the approach described herein must be changed if it is to be used to investigate damped beams.

Funding Acknowledgement

'This research received no specific grant from any funding agency in the public, commercial, or not-for-profit sectors'.

Conflict of interest statement

'The authors declare no conflict of interest in preparing this article'.

References

Ahmed, N., Uddin, M.K., 2019. Vibration analysis of a Cracked I beam subjected to periodic load.

Aria, A.I., Friswell, M.I., Rabczuk, T., 2019. Thermal vibration analysis of cracked nanobeams embedded in an elastic matrix using finite element analysis. *Composite Structures* 212, 118–128. doi:https://doi.org/10.1016/j.compstruct.2019.01.040.

Banerjee, J.R., Guo, S., 2009. On the Dynamics of Cracked Beams. American Institute of Aeronautics and Astronautics. Structures, Structural Dynamics, and Materials and Co-located Conferences. doi:doi:10.2514/6.2009-2429.

Bickford, W.B., 1982. A consistent higher order beam theory. Classification: 001B: Physique / Physics Inist-CNRS record number PASCAL83X0184967.

Bozyigit, B., Yesilce, Y., 2016. Dynamic stiffness approach and differential transformation for free vibration analysis of a moving reddy-bickford beam. *Structural Engineering and Mechanics* 58, 847–868. doi:10.12989/SEM.2016.58.5.847.

Caddemi, S., Caliò, I., 2009. Exact closed-form solution for the vibration modes of the euler–bernoulli beam with multiple open cracks. *Journal of Sound and Vibration* 327, 473–489. doi:doi:10.1016/j.jsv.2009.07.008.

Caddemi, S., Caliò, I., 2013. The exact explicit dynamic stiffness matrix of multi-cracked euler–bernoulli beam and applications to damaged frame structures. *Journal of Sound and Vibration* 332, 3049–3063. doi:doi:10.1016/j.jsv.2013.01.003.

Caddemi, S., Calio, I., Cannizzaro, F., 2017. The dynamic stiffness matrix (dsm) of axially loaded multi-cracked frames. *Mechanics Research Communications* 84, 90–97. doi:https://doi.org/10.1016/j.mechrescom.2017.06.012.

Caddemi, S., Morassi, A., 2013. Multi-cracked euler–bernoulli beams: Mathematical modeling and exact solutions. *International Journal of Solids and Structures* 50, 944–956. doi:doi:10.1016/j.ijsolstr.2012.11.018.

Cheng, Y., Yu, Z., Wu, X., Yuan, Y., 2011. Vibration analysis of a cracked rotating tapered beam using the p-version finite element method. *Finite Elements in Analysis and Design* 47, 825–834.

Cowper, G.R., 1966. The shear coefficient in timoshenko's beam theory. *Journal of Applied Mechanics* 33, 335–340. doi:doi:10.1115/1.3625046.

Şimeşk, M., Kocatürk, T., 2007. Free vibration analysis of beams by using a third-order shear deformation theory. *Sadhana* 32, 167–179. doi:doi:10.1007/s12046-007-0015-9.

Dilena, M., Dell'Oste, M.F., Morassi, A., 2011. Detecting cracks in pipes filled with fluid from changes in natural frequencies. *Mechanical Systems and Signal Processing* 25, 3186–3197. doi:doi:10.1016/j.ymssp.2011.04.013.

Dimarogonas, A.D., 1996. Vibration of cracked structures: A state of the art review. *Engineering Fracture Mechanics* 55, 831–857. doi:doi:10.1016/0013-7944(94)00175-8.

Dwivedi, S.K., Vishwakarma, M., Soni, P.A., 2018. Advances and researches on non destructive testing: A review. *Materials Today: Proceedings* 5, 3690–3698. doi:doi:10.1016/j.matpr.2017.11.620.

Ebrahimi, A., Meghdari, A., Behzad, M., 2005. A new approach for vibration analysis of a cracked beam. *International Journal of Engineering* 18, 319–330.

El-Sayed, T., Hand, R.J., 2011. Modelling the strengthening of glass using epoxy based coatings. *Journal of the European Ceramic Society* 31, 2783–2791. doi:doi:10.1016/j.jeurceramsoc.2011.05.033.

El-Sayed, T.A., El-Mongy, H.H., 2021. A new numeric-symbolic procedure for variational iteration method with application to the free vibration of generalized multi-span timoshenko beam. *Journal of Vibration and Control* -, 1–13.

El-Sayed, T.A., Farghaly, S.H., 2018. Frequency equation using new set of fundamental solutions with application on the free vibration of timoshenko beams with intermediate rigid or elastic span. *Journal of Vibration Control* 24, 4764–4780.

El-Sayed, T.A., Farghaly, S.H., 2020. Formulae for the frequency equations of beam-column system carrying a fluid storage tank. *Structural Engineering and Mechanics* 73, 83–95. doi:doi:sem.2020.73.1.083.

Elsawaf, A., El-sayed, T.A., Farghaly, S.H., 2020. Optimal design for maximum fundamental frequency and minimum intermediate support stiffness for uniform and stepped beams composed of different materials. doi:https://doi.org/10.4271/2020-01-5014.

Farghaly, S., El-Sayed, T., 2016. Exact free vibration of multi-step timoshenko beam system with several attachments. *Mechanical Systems and Signal Processing* 72, 525–546.

Farghaly, S.H., 1994. Vibration and stability analysis of timoshenko beams with discontinuities in cross-section. *Journal of Sound and Vibration* 174, 591–605. doi:doi:10.1006/jsvi.1994.1296.

Farghaly, S.H., El-Sayed, T.A., 2017. Exact free vibration analysis for mechanical system composed of timoshenko beams with intermediate eccentric rigid body on elastic supports: An experimental and analytical investigation. *Mechanical Systems and Signal Processing* 82, 376–393.

Friswell, M.I., 2007. Damage identification using inverse methods. *Philosophical Transactions of the Royal Society A: Mathematical, Physical and Engineering Sciences* 365, 393–410. doi:doi:10.1098/rsta.2006.1930.

Heyliger, P.R., Reddy, J.N., 1988. A higher order beam finite element for bending and vibration problems. *Journal of Sound and Vibration* 126, 309–326. doi:doi:10.1016/0022-460X(88)90244-1.

Huang, Y., Wu, J.X., Li, X.F., Yang, L.E., 2013. Higher-order theory for bending and vibration of beams with circular cross section. *Journal of Engineering Mathematics* 80, 91–104. doi:doi:10.1007/s10665-013-9620-2.

Jemielita, G., 1975. Technical theory of plates with moderate thickness. *Rozprawy Ink* 23, 483–499.

Jun, L., Xiaobin, L., Hongxing, H., 2009. Free vibration analysis of third-order shear deformable composite beams using dynamic stiffness method. *Archive of Applied Mechanics* 79, 1083–1098. doi:doi:10.1007/s00419-008-0276-8.

Karamanlı, A., 2018. Free vibration analysis of two directional functionally graded beams using a third order shear deformation theory. *Composite Structures* 189, 127–136. doi:doi:10.1016/j.compstruct.2018.01.060.

Kaya, Y., Dowling, J., 2016. Application of timoshenko beam theory to the estimation of structural response. *Engineering Structures* 123, 71–76. doi:doi:10.1016/j.engstruct.2016.05.026.

Khdeir, A.A., Reddy, J.N., 1994. Free vibration of cross-ply laminated beams with arbitrary boundary conditions. *International Journal of Engineering Science* 32, 1971–1980. URL: http://www.sciencedirect.com/science/article/pii/0020722594900930, doi:doi:10.1016/0020-7225(94)90093-0.

Kim, K., Kim, S., Sok, K., Pak, C., Han, K., 2018. A modeling method for vibration analysis of cracked beam with arbitrary boundary condition. *Journal of Ocean Engineering and Science* 3, 367–381. doi:doi:10.1016/j.joes.2018.11.003.

Kisa, M., Brandon, J., Topcu, M., 1998. Free vibration analysis of cracked beams by a combination of finite elements and component mode synthesis methods. *Computers & Structures* 67, 215–223. doi:doi:10.1016/S0045-7949(98)00056-X.

Labib, A., Kennedy, D., Featherston, C., 2014. Free vibration analysis of beams and frames with multiple cracks for damage detection. *Journal of Sound and Vibration* 333, 4991–5003. doi:doi:10.1016/j.jsv.2014.05.015.

Levinson, M., 1980. An accurate, simple theory of the statics and dynamics of elastic plates. *Mechanics Research Communications* 7, 343–350. doi:doi:10.1016/0093-6413(80)90049-X.

Levinson, M., 1981. A new rectangular beam theory. *Journal of Sound and Vibration* 74, 81–87. doi:doi:10.1016/0022-460X(81)90493-4.

Loya, J., López-Puente, J., Zaera, R., Fernández-Sáez, J., 2009. Free transverse vibrations of cracked nanobeams using a nonlocal elasticity model. *Journal of Applied Physics* 105, 044309. doi:doi:10.1063/1.3068370.

Luo, H., Hanagud, S., 1997. An integral equation for changes in the structural dynamics characteristics of damaged structures. *International Journal of Solids and Structures* 34, 4557–4579. doi:doi:10.1016/S0020-7683(97)00038-3.

Marur, S.R., Kant, T., 1996. Free vibration analysis of fiber reinforced composite beams using higher order theories and finite element modelling. *Journal of Sound and Vibration* 194, 337–351. doi:doi:10.1006/jsvi.1996.0362.

Mazaheri, H., Rahami, H., Kheyroddin, A., 2018. Static and dynamic analysis of cracked concrete beams using experimental study and finite element analysis. *Periodica Polytechnica Civil Engineering* 62, 337–345. doi:doi:10.3311/PPci.11450.

Morassi, A., 2001. Identification of a crack in a rod based on changes in a pair of natural frequencies. *Journal of Sound and Vibration* 242, 577–596. doi:doi:10.1006/jsvi.2000.3380.

Patil, D.P., Maiti, S.K., 2005. Experimental verification of a method of detection of multiple cracks in beams based on frequency measurements. *Journal of Sound and Vibration* 281, 439–451. doi:doi:10.1016/j.jsv.2004.03.035.

Reddy, J.N., 1984a. Energy and variational methods in applied mechanics: with an introduction to the finite element method. Wiley New York.

Reddy, J.N., 1984b. A simple higher-order theory for laminated composite plates. *Journal of Applied Mechanics* 51, 745–752. doi:doi:10.1115/1.3167719.

Sánchez, P.S., Negro, P.L., García-Fogeda, P., 2016. Vibration-based method for damage detection at welded beams and rods. *Latin American Journal of Solids and Structures* 13, 2336–2355.

Soldatos, K.P., Sophocleous, C., 2001. On shear deformable beam theories: the frequency and normal mode equations of the homogeneous orthotropic bickford beam. *Journal of Sound and Vibration* 242, 215–245. doi:doi:10.1006/jsvi.2000.3367.

Timoshenko, S.P., 1921. Lxvi. on the correction for shear of the differential equation for transverse vibrations of prismatic bars. *The London, Edinburgh, and Dublin Philosophical Magazine and Journal of Science* 41, 744–746. doi:doi:10.1080/14786442108636264.

Torabi, K., Nafar Dastgerdi, J., 2012. An analytical method for free vibration analysis of timoshenko beam theory applied to cracked nanobeams using a nonlocal elasticity model. *Thin Solid Films* 520, 6595–6602. doi:doi:10.1016/j.tsf.2012.06.063.

Vestroni, F., Capecchi, D., 2000. Damage detection in beam structures based on frequency measurements. *Journal of Engineering Mechanics* 126, 761–768. doi:doi:10.1061/(ASCE)0733-9399(2000)126:7(761).

Wang, C.M., Reddy, J.N., Lee, K.H., 2000. Chapter 2 - Bending of Beams. Elsevier Science Ltd, Oxford. pp. 11–38. doi:doi:10.1016/B978-008043784-2/50002-2.

Wattanasakulpong, N., Chaikittiratana, A., Pornpeerakeat, S., 2018. Chebyshev collocation approach for vibration analysis of functionally graded porous beams based on third-order shear deformation theory. *Acta Mechanica Sinica* 34, 1124–1135. doi:doi:10.1007/s10409-018-0770-3.

Xiaoqing, Z., Qiang, H., Feng, L., 2010. Analytical approach for detection of multiple cracks in a beam. *Journal of Engineering Mechanics* 136, 345–357. doi:doi:10.1061/(ASCE)0733-9399(2010)136:3(345).

Yamuna, P., Sambasivarao, K., 2014. Vibration analysis of beam with varying crack location. *International Journal of Engineering Research and General Science* 2, 1008–1017.

Yang, E.C., Zhao, X., Li, Y.H., 2015. Free vibration analysis for cracked fgm beams by means of a continuous beam model. *Shock and Vibration* 2015, 197049. doi:doi:10.1155/2015/197049.

Yardimoglu, B., 2010. A novel finite element model for vibration analysis of rotating tapered timoshenko beam of equal strength. *Finite Elem. Anal. Des.* 46, 838–842.

Yendhe, V.S., Kadlag, P., SHELKE, P., 2016. Vibration analysis of cracked cantilever beam for varying crack size and location. *International Research Journal of Engineering and Technology* 3, 1913–1919.

Yesilce, Y., 2011. Free vibrations of a reddy-bickford multi-span beam carrying multiple spring-mass systems. *Shock and Vibration* 18, 709–726. doi:doi:10.3233/SAV-2010-0593.

Yesilce, Y., Catal, H.H., 2011. Solution of free vibration equations of semi-rigid connected reddy-bickford beams resting on elastic soil using the differential transform method. *Archive of Applied Mechanics* 81, 199–213. doi:doi:10.1007/s00419-010-0405-z.

Yesilce, Y., Catal, S., 2009. Free vibration of axially loaded reddy-bickford beam on elastic soil using the differential transform method. *Struct. Eng. Mech* 31, 453–476. doi:doi:10.12989/sem.2009.31.4.453.

Appendix A. Elements of stiffness and mass matrix

The finite element equation of any elements without attachments may be written as

$$\begin{bmatrix} [K^{11}] & [K^{12}] \\ [K^{21}] & [K^{22}] \end{bmatrix} - \omega^2 \begin{bmatrix} [M^{11}] & [M^{12}] \\ [M^{21}] & [M^{22}] \end{bmatrix} \begin{Bmatrix} \{\Delta\} \\ \{\psi\} \end{Bmatrix} = \begin{Bmatrix} F^1 \\ F^2 \end{Bmatrix}, \tag{A.1}$$

where

$$
\begin{aligned}
K_{ij}^{11} &= \int_0^L \left[\frac{1}{21} EI \frac{d^2H_i}{dx^2} \frac{d^2H_j}{dx^2} + \frac{8}{15} GA \frac{dH_i}{dx} \frac{dH_j}{dx} \right] dx, \\
K_{ij}^{12} &= \int_0^L \left[-\frac{16}{105} EI \frac{d^2H_i}{dx^2} \frac{dL_j}{dx} + \frac{8}{15} GA \frac{dH_i}{dx} L_j \right] dx = K_{ji}^{21}, \\
K_{ij}^{22} &= \int_0^L \left[\frac{68}{105} EI \frac{dL_i}{dx} \frac{dL_j}{dx} + \frac{8}{15} GA \, L_i L_j \right] dx, \\
M_{ij}^{11} &= \int_0^L \left[\frac{1}{21} \rho I \frac{dH_i}{dx} \frac{dH_j}{dx} + \rho A H_i H_j \right] dx, \\
M_{ij}^{12} &= \int_0^L \left[-\frac{16}{105} \rho I \, \frac{dH_i}{dx} L_j \right] dx = M_{ji}^{21}, \\
M_{ij}^{22} &= \int_0^L \left[\frac{68}{105} \rho I \, L_i L_j \right] dx, \\
F_i^1 &= \int_0^L [f \, H_i] \, dx, \\
F_i^2 &= 0.
\end{aligned}
$$

The stiffness and mass matrices and force vector are rearranged according to the displacement vector $\mathbf{\Delta}_e = \{w_1 \; \theta_1 \; \psi_1 \; w_2 \; \theta_2 \; \psi_2\}$ as:

$$
\mathbf{K}_e = \frac{2 \, E \, I}{105 \, l^3} \begin{bmatrix}
30 & -15l & 0 & -30 & -15l & 0 \\
-15l & 10l^2 & 8l^2 & 15l & 5l^2 & -8l^2 \\
0 & 8l^2 & 34l^2 & 0 & -8l^2 & -34l^2 \\
-30 & 15l & 0 & 30 & 15l & 0 \\
-15l & 5l^2 & -8l^2 & 15l & 10l^2 & 8l^2 \\
0 & -8l^2 & -34l^2 & 0 & 8l^2 & 34l^2
\end{bmatrix} + \tag{A.2}
$$

$$
\frac{8 \, G \, A}{15} \begin{bmatrix}
\frac{1.2}{l} & -0.1 & -0.5 & -\frac{1.2}{l} & -0.1 & -0.5 \\
-0.1 & \frac{2 \, l}{15} & -\frac{l}{12} & 0.1 & -\frac{l}{30} & \frac{l}{12} \\
-0.5 & -\frac{l}{12} & \frac{l}{3} & 0.5 & \frac{l}{12} & \frac{l}{6} \\
-\frac{1.2}{l} & 0.1 & 0.5 & \frac{1.2}{l} & 0.1 & 0.5 \\
-0.1 & -\frac{l}{30} & \frac{l}{12} & 0.1 & \frac{2 \, l}{15} & -\frac{l}{12} \\
-0.5 & \frac{l}{12} & \frac{l}{6} & 0.5 & -\frac{l}{12} & l/3
\end{bmatrix}
$$

$$\mathbf{M_e} = \frac{\rho\, A\, l}{420}\begin{bmatrix} 156 & -22\,l & 0 & 54 & 13\,l & 0 \\ -22\,l & 4\,l^2 & 0 & -13\,l & -3\,l^2 & 0 \\ 0 & 0 & 0 & 0 & 0 & 0 \\ 54 & -13\,l & 0 & 156 & 22\,l & 0 \\ 13\,l & -3\,l^2 & 0 & 22\,l & 4\,l^2 & 0 \\ 0 & 0 & 0 & 0 & 0 & 0 \end{bmatrix} + \tag{A.3}$$

$$+\frac{\rho\, I}{630\,l}\begin{bmatrix} 36 & -3\,l & 48\,l & -36 & -3\,l & 48\,l \\ -3\,l & 4\,l^2 & 8\,l^2 & 3\,l & -l^2 & -8\,l^2 \\ 48\,l & 8\,l^2 & 136\,l^2 & -48\,l & -8\,l^2 & 68\,l^2 \\ -36 & 3\,l & -48\,l & 36 & 3\,l & -48\,l \\ -3\,l & -l^2 & -8\,l^2 & 3\,l & 4\,l^2 & 8\,l^2 \\ 48\,l & -8\,l^2 & 68\,l^2 & -48\,l & 8\,l^2 & 136\,l^2 \end{bmatrix}$$

$$\mathbf{F}_e = \begin{Bmatrix} \frac{fl}{2} \\ -\frac{fl^2}{12} \\ 0 \\ \frac{fl}{2} \\ \frac{fl^2}{12} \\ 0 \end{Bmatrix} \tag{A.4}$$

l is the element length.